North Atlantic surface water mass transformation contributions to AMOC in eddy-parameterized and eddy-resolving simulations

Ben Moore-Maley[1], Julie McClean[2], Sarah Gille[2], Alice Barthel[1], Luke Van Roekel[1]

[1]Los Alamos National Laboratory, Los Alamos, New Mexico [2]Scripps Institution of Oceanography/University of California San Diego, La Jolla, California

Contact: bmoorema@lanl.gov

Scan for pdf with references

OS11D-0707
Monday, December 9
8:30-12:20

Motivation

The Atlantic Meridional Overturning Circulation (AMOC) is an important component of the global climate system. Surface water mass transformation in the subpolar North Atlantic preconditions the deep water formation that contributes to the deep equatorward branch of AMOC. Surface transformation is thus a valuable diagnostic for interpreting observations of overturning circulation and evaluating model AMOC performance.

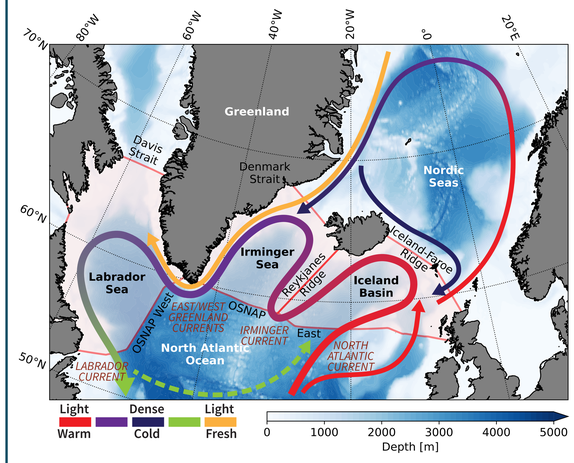

Figure 1 Map of the subpolar North Atlantic showing bathymetry, study regions and subpolar gyre circulation. Regions are bounded equatorward by the Overturning in the Subpolar North Atlantic Program (OSNAP) observing lines (Lozier et al., 2019).

Research question

How does surface water mass transformation contribute to subpolar overturning circulation in an eddy-parameterized vs. eddy-resolving ocean simulation?

Key points

1. Water mass analysis in temperature-salinity (TS) coordinates can be a powerful diagnostic for evaluating ocean model AMOC performance.
2. In the eddy-parameterized (LR) simulation presented here, an early surface freshwater bias suppresses surface transformation in the Irminger and Labrador Seas
3. This suppressed transformation is accompanied by poorly-formed TS properties of the subpolar gyre boundary currents.

Method

Surface water mass transformation is based on the Walin (1982) framework.

(1) Density transformation*

$$Tr(\rho) = -\frac{1}{\Delta\rho}\iint_A \left[\frac{\alpha H_{net}}{C_p} + \beta S F_{net}\right] \times \sqcap\left[\rho, \rho'(x,y)\right]\, dA$$

Bin size | Heat flux component | Freshwater flux component | Binning function

(2) Temperature transformation**

$$Tr(T) = \frac{1}{\Delta T}\iint_A \frac{H_{net}}{\rho' C_p} \times \sqcap\left[T, T'(x,y)\right]\, dA$$

(3) Salinity transformation**

$$Tr(S) = -\frac{1}{\Delta S}\iint_A S' F_{net} \times \sqcap\left[S, S'(x,y)\right]\, dA$$

*Speer and Tziperman (1992), **Evans et al. (2014)

Simulations

DOE Energy Exascale Earth System Model (E3SM) (Golaz et al., 2022)

- Forced configurations with coupled ocean and sea ice components
  - Model for Prediction Across Scales (MPAS-Ocean, MPAS-Seaice)
- Unstructured hexagonal mesh, allows regional resolution refinement

Configurations

- Low Resolution (LR), 30-60 km
  - Gent and McWilliams (1990) + Redi (1982) mesoscale eddy parameterizations
- High Resolution (HR), 6-18 km
  - mesoscale eddy resolving

Forcing and initialization

- Coordinated Ocean-ice Reference Experiments II (CORE-II) protocol (1948-2009) (Large and Yeager, 2009)
- Polar Science Center Hydrographic Climatology (PHC2) initialization (Steele et al., 2001)

AMOC

- **AMOC weakens from the initial state in the LR simulation over the first 10 years**

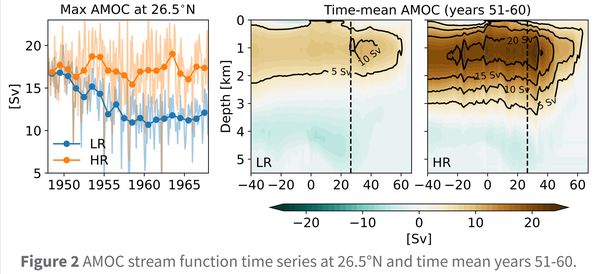

Figure 2 AMOC stream function time series at 26.5°N and time mean years 51-60.

Early simulation adjustment

- **LR: surface freshening, mixed layer shoaling, and westward subpolar gyre shift**

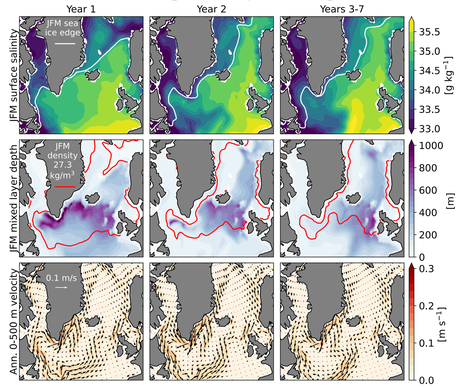

Figure 3 Low Resolution (LR): Jan-Mar (JFM) surface salinity, JFM mixed layer depth, and annual 0-500 m velocity fields for years 1, 2, and 3-7. JFM sea ice extent (white) and 27.3 kg m^{-3} surface density (red) also shown.

- **HR: no significant adjustment, except Greenland Sea mixed layer deepening**

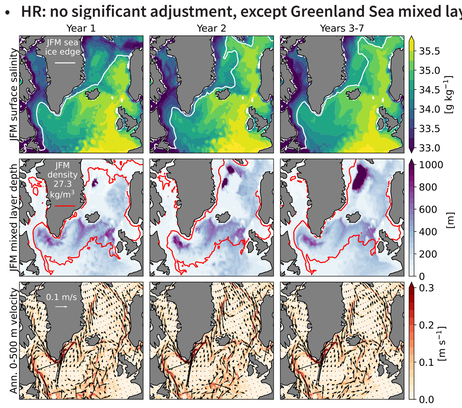

Figure 4 As in Figure 3, but for the High Resolution (HR) simulation.

Adjusted state at the OSNAP line

- **Depressed isopycnals following LR freshening adjustment**

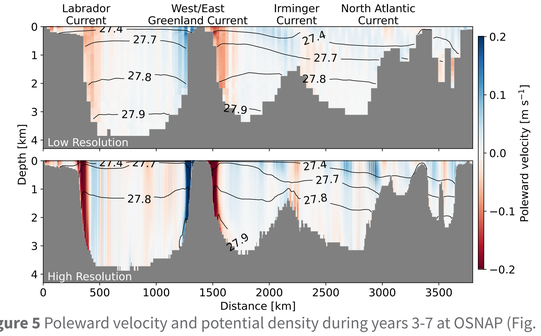

Figure 5 Poleward velocity and potential density during years 3-7 at OSNAP (Fig. 1).

Surface density transformation

- **At higher densities, surface transformation is increasingly present in the Irminger and Labrador Seas at HR, but not at LR**

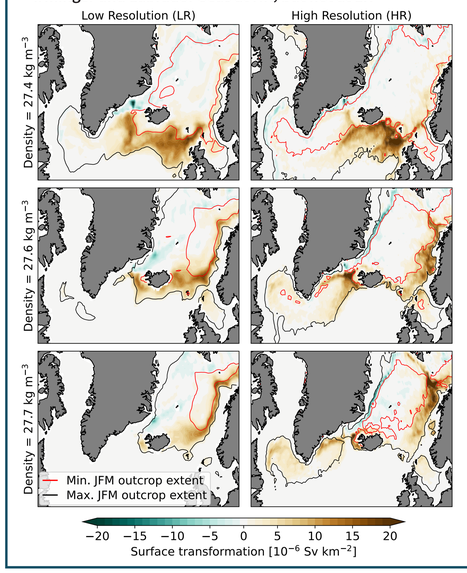

Figure 6 Surface density transformation maps (integrand of Eq. 1) at three potential density bins during years 3-7. Min/max JFM surface outcrops are also shown for each density bin.

TS transformation and overturning

- **In both simulations, transformation proceeds from warm/salty (Iceland Basin) to cold/fresh (Labrador Sea)**
- **Transformation is present between 27.6 and 27.8 kg m^{-3} at HR, but not at LR**
- **This transformation accompanies a robust Labrador Sea Water export at HR**

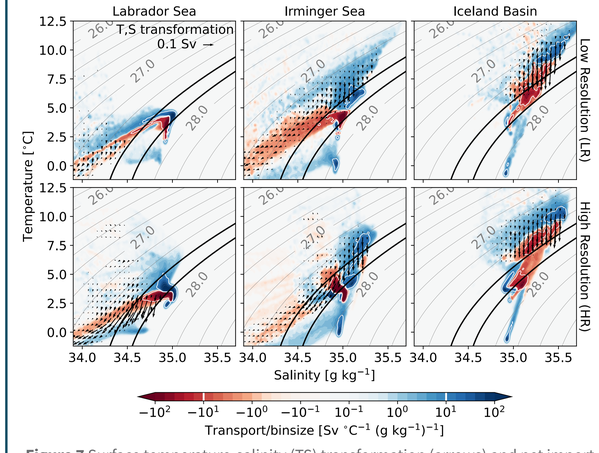

Figure 7 Surface temperature-salinity (TS) transformation (arrows) and net import (blue) and export (red) transports by region (years 3-7). Potential density in gray.

References

Evans, D. G., J. D. Zika, A. C. Naveira Garabato, and A. J. G. Nurser (2014), The imprint of Southern Ocean overturning on seasonal water mass variability in Drake Passage, *JGR Oceans*, 119, 7987-8010. https://doi.org/10.1002/2014JC010097

Gent, P. R. and J. C. McWilliams (1990), Isopycnal mixing in ocean circulation models, *JPO*, 20, 150-155. https://doi.org/10.1175/1520-0485(1990)020<0150:IMIOCM>2.0.CO;2

Golaz, J.-C., L. P. Van Roekel, X. Zheng, A. F. Roberts, J. D. Wolfe, W. Lin, et al. (2022), The DOE E3SM Model version 2: Overview of the physical model and initial model evaluation, *JAMES*, 14, e2022MS003156. https://doi.org/10.1029/2022MS003156

Large, W. G. and S. G. Yeager (2009), The global climatology of an interannually varying air-sea flux data set, *Clim. Dyn.*, 33, 341-364. https://doi.org/10.1007/s00382-008-0441-3

Lozier, M. S., F. Li, S. Bacon, F. Bahr, A. S. Bower, S. A. Cunningham, et al. (2019), A sea change in our view of overturning in the subpolar North Atlantic, *Science*, 363, 516–521. https://doi.org/10.1126/science.aau6592

Redi, M. H. (1982), Oceanic isopycnal mixing by coordinate rotation, *JPO*, 12, 1154-1158. https://doi.org/10.1175/1520-0485(1982)012<1154:OIMBCR>2.0.CO;2

Speer, K. and E. Tziperman (1992), Rates of water mass formation in the North Atlantic Ocean, *JPO*, 22, 93-104. https://doi.org/10.1175/1520-0485(1992)022<0093:ROWMFI>2.0.CO;2

Steele, M., R. Morley, and W. Ermold (2001), PHC: A global ocean hydrography with a high-quality Arctic Ocean, *J. Clim.*, 14, 2079-2087. https://doi.org/10.1175/1520-0442(2001)014<2079:PAGOHW>2.0.CO;2

Walin, G. (1982), On the relation between sea-surface heat flow and thermal circulation in the ocean, *Tellus*, 34, 187-195. https://doi.org/10.1111/j.2153-3490.1982.tb01806.x

Los Alamos National Laboratory | UC San Diego | Scripps Institution of Oceanography | U.S. Department of Energy, Office of Science | ImPACTS | E3SM Energy Exascale Earth System Model

LA-UR-24-32849